ELSEVIER

Catalysis Today 78 (2003) 303–310

CATALYSIS TODAY

www.elsevier.com/locate/cattod

Phase transformations in mesostructured vanadium–phosphorus-oxides

Moises A. Carreon, Vadim V. Guliants*

Department of Chemical Engineering, University of Cincinnati, Cincinnati, OH 45221-0171, USA

Abstract

Mesostructured lamellar, hexagonal and cubic vanadium–phosphorus-oxide (VPO) phases were prepared employing cationic, anionic and alkylamine surfactants under mild conditions and low pH. The obtained mesophases displayed desirable vanadium oxidation states (+3.8 to +4.3) and P/V molar ratios ∼1.0 for the partial oxidation of *n*-butane to maleic anhydride. As-synthesized mesostructured VPO underwent phase transformations to various mesostructured and dense VPO phases depending on the post-synthesis treatment. The phase transformations of mesostructured VPO during Soxhlet extraction and thermal treatment in N_2 have been observed for the first time. These transformations were explained by the changes in the surfactant packing parameter, *g*. Calcination in air produced more disordered mesostructures and dense VPO phases such as γ-$VOPO_4$ and $(VO)_2P_2O_7$.
© 2002 Elsevier Science B.V. All rights reserved.

Keywords: Mesostructured VPO; Post-synthesis treatment; Mesophase transformations; Dense phases; Packing parameter

1. Introduction

Vanadium-containing mixed metal oxides possess highly promising catalytic properties for the selective oxidation of lower alkanes [1]. For example, Mo–V–Nb and Sb–V oxides are catalytically active in the oxidative dehydrogenation and selective oxidation of ethane and ammoxidation of propane [2,3]. The vanadium–phosphorus-oxide (VPO) is the only commercial catalytic system for selective oxidation of *n*-butane to maleic anhydride [4,5]. However, the current synthesis approaches for the VPO system offer a limited control over structural and compositional parameters that define its catalytic performance in oxidation catalysis. Self-assembly routes are highly promising for the molecular design of mixed metal oxides with desirable structural, compositional and catalytic properties. The discovery of M41S family of silicate mesoporous molecular sieves [6,7] has stimulated the search for structurally similar non-silicate materials with diverse compositions [8]. Although several mesostructured transition metal oxides (e.g. Sb [9], Mo [10] and V [11]) have been reported, these phases suffer from limited thermal stability. Only a few publications exist on the synthesis of mesostructured mixed metal oxides, all with VPO compositions [12–15]. Iwamoto and coworkers [12] reported the synthesis of mesostructured hexagonal VPO materials using alkyltrimethyl ammonium surfactants (C_{12}–C_{16}). Doi and Miyake [13] prepared a hexagonal mesostructured VPO phase from the catalyst precursor, $VOHPO_4{\cdot}0.5H_2O$, by surfactant intercalation and a subsequent hydrothermal treatment. Amoros and coworkers [14] described the synthesis of hexagonal mesostructured oxovanadium phosphates, denoted as ICMUV-2. Recently, Mizuno et al. [15] obtained

* Corresponding author. Tel.: +1-513-556-0203; fax: +1-513-556-3473.
E-mail address: vadim.guliants@uc.edu (V.V. Guliants).

0920-5861/02/$ – see front matter © 2002 Elsevier Science B.V. All rights reserved.
PII: S0920-5861(02)00314-0

hexagonal, cubic and lamellar mesostructured VPOs. However, the structural order in all these materials was lost upon calcination, and in some cases [12,13] the P/V compositions obtained were not optimal for selective butane oxidation. We describe here novel "soft chemistry" approaches to mesostructured VPO which provide improved thermal stability, desirable P/V compositions and vanadium oxidation states for the partial oxidation of *n*-butane.

2. Experimental

2.1. Materials

$VOSO_4$ (Aldrich), H_3PO_3 and H_3PO_4 (85%) (Fisher Chemicals) were used as the VPO sources. The synthesis pH was adjusted with NH_4OH and HCl (Fisher Chemicals). The following cationic, anionic and neutral surfactants were employed in the synthesis: alkyltrimethyl ammonium bromides, $CH_3(CH_2)_n N(CH_3)_3Br$, $n = 11, 13, 15, 17$ (Aldrich); monododecyl phosphate, $CH_3(CH_2)_{11}OPO(OH)_2$ (Lancaster); sodium hexadecane sulphonate, $CH_3(CH_2)_{15}SO_3Na$ (Lancaster); dodecyl sodium sulfate salt, $CH_3(CH_2)_{11} OSO_3Na$ (Aldrich); primary alkylamines, $CH_3(CH_2)_n NH_2$, $n = 11, 15, 17$ (Lancaster).

2.2. Synthesis

Lamellar, hexagonal and cubic VPO phases were prepared under mild conditions by reacting aqueous solutions containing vanadium ($VOSO_4$) and phosphorus (H_3PO_3 or H_3PO_4) sources in the presence of surfactants. In a typical synthesis, an aqueous solution containing the phosphorus and vanadium sources was added to an aqueous surfactant solution. The pH of the resultant solution was adjusted with HCl (1 M) to below 1.0. The typical synthesis compositions were (on molar basis): H_2O/surfactant = 300–525, surfactant/V = 0.6–1.1. The P/V molar ratio was kept constant at 1.1, which is the optimal bulk composition for the partial oxidation of *n*-butane. The obtained sol was homogenized by stirring for 6 h at 343 K, precipitated with NH_4OH at $2.5 < pH < 4.0$, and stirred for an additional 24 h. The resultant slurry was filtered, washed with deionized water, and dried overnight at 373 K. The as-synthesized mesophases were treated in air or nitrogen at 673 K for 6 h (3 °C/min). Alternatively, the surfactant was removed by Soxhlet extraction with ethanol.

2.3. Characterization

Powder X-ray diffraction (XRD) patterns were recorded on a Siemens D-500 spectrometer using Cu Kα radiation with a step size of 0.02°/s. Transmission electron microscopy study was conducted using a JEOL-2010F microscope. Scanning electron micrographs were recorded on a Hitachi S-3200N SEM. The average oxidation state of vanadium was determined by a double titration method [16]. The XPS analysis was performed using a model DS800 XPS surface analysis system. P/V ratios were determined by ICP (Thermo Jarrell Ash ICAP 1100). The BET specific surface areas were determined using a Micromeritics Gemini 2360 analyzer.

3. Results and discussion

3.1. As-synthesized VPO mesophases

Fig. 1 shows typical XRD patterns for these novel mesophases. Fig. 1a shows the XRD pattern

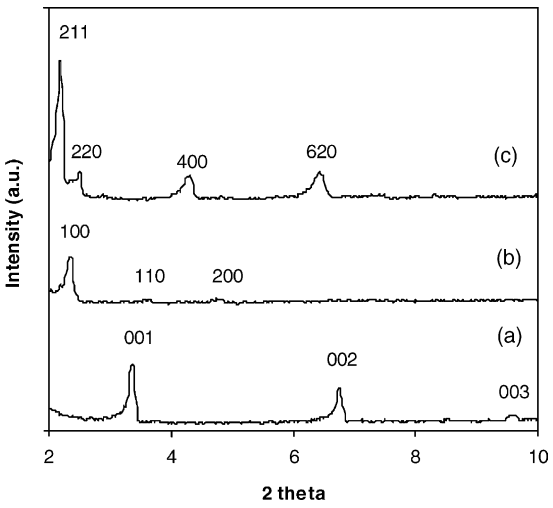

Fig. 1. XRD patterns of as-synthesized (a) lamellar, (b) hexagonal and (c) cubic mesoporous VPO phases prepared using $CH_3(CH_2)_{15}(CH_3)_3Br$, $CH_3(CH_2)_{11}NH_2$ and $CH_3(CH_2)_{15}SO_3Na$ as surfactants, respectively.

of mesostructured VPO (meso-VPO) prepared using cetyltrimethyl ammonium bromide as surfactant. Three strong reflections were observed at $2\theta = 3.36^\circ$, 6.75° and 9.77° corresponding to the (0 0 1), (0 0 2) and (0 0 3) planes of the lamellar structure, respectively. Fig. 1b shows the XRD pattern of meso-VPO synthesized using dodecylamine as surfactant. Three strong reflections were observed at $2\theta = 2.32^\circ$, 3.58° and 4.76° corresponding to the (1 0 0), (1 1 0) and (2 0 0) planes of the hexagonal structure, respectively. The XRD pattern of meso-VPO synthesized with sodium hexadecane sulphonate as surfactant is shown in Fig. 1c. This sample showed the presence of four strong reflections at $2\theta = 2.17^\circ$, 2.47°, 4.29° and 6.44° corresponding to the (2 1 1), (2 2 0), (4 0 0), and (6 2 0) planes of the cubic structure, respectively [15,17]. In all the cases, no other reflections were observed in the $10^\circ < 2\theta < 30^\circ$ range indicating the formation of a single mesophase.

Fig. 2 shows the TEM image of hexagonal meso-VPO prepared using mirystyltrimethyl ammonium bromide as a surfactant displaying a highly ordered hexagonal array of cylindrical ~28 Å pores. Fig. 3 shows representative SEM images for as-synthesized meso-VPO. Fig. 3a shows the plate-like type morphology of lamellar VPO phase. This phase was made up of large aggregates of crystalline platelets with an average size of 1–8 μm. The sheet-disk morphology of hexagonal meso-VPO is shown in Fig. 3b. This phase consisted of flat particles 8–12 μm wide and ~0.5 μm thick. Similar sheet and plate-like morphologies for hexagonal mesostructured oxovanadium phosphates were observed by Amoros and coworkers [14]. Fig. 3c shows the morphology of cubic meso-VPO. This phase consisted mainly of ellipsoidal 15–20 μm particles. The hexagonal and cubic meso-VPO phases displayed more significant surface curvature (disks and ellipsoids) than the lamellar phases (platelets). This behavior may be rationalized in terms of the surfactant packing parameter "*g*" [18].The packing parameter is defined as $g = V/a_0 l$, where a_0 is the surfactant headgroup area at the interface, V the total volume of the surfactant plus any cosolvent molecules between the chains, and l the surfactant chain length. For $1/3 < g < 1/2$, the formation of hexagonal phases is favored. For $1/2 < g < 2/3$, the cubic phases are preferred, and for $g = 1$ the lamellar phases are observed. Small values of "*g*" favor high surface curvature encountered in hexagonal or cubic phases, while large values lead only to lamellar phases with low surface curvature.

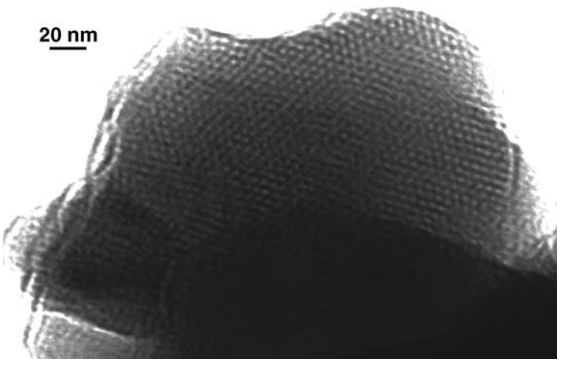

Fig. 2. TEM image of as-synthesized mesoporous VPO prepared using $CH_3(CH_2)_{13}N(CH_3)_3Br$ as a surfactant.

3.2. Phase transformations of mesostructured VPO

Soxhlet-extraction. The surfactants may be removed by Soxhlet extraction with ethanol. Extraction is a more gentle, less invasive surfactant removal technique than calcination, because it better preserves the original mesostructure. Fig. 4 shows the XRD patterns for as-synthesized and Soxhlet-extracted mesostructured VPO phases obtained using monododecyl phosphate as a template. The as-synthesized sample (Fig. 4a) shows three reflections at $2\theta = 2.41^\circ$, 4.88° and 7.20° corresponding to the (1 0 0), (2 0 0) and (2 1 0) planes of the hexagonal phase, respectively. Interestingly, after Soxhlet extraction with ethanol for 3 days (Fig. 4b), the sample displayed the characteristic reflections of the cubic mesophase at $2\theta = 2.20^\circ$, 3.10°, 4.37° and 6.13° corresponding to the (2 1 1), (2 2 0), (4 2 0) and (6 2 0) planes of the cubic mesostructure, respectively. The hexagonal-to-cubic phase transformation may be explained by the changes in the packing parameter *g* [18]. Stucky and coworkers [19–21] have shown that small alcohol molecules tend to reside primarily in the outer shell of the surfactant micelle increasing the effective surfactant volume (*V*). Therefore, the presence of ethanol during Soxhlet extraction process increased *V*, raising the value of the surfactant packing parameter and causing the hexagonal-to-cubic transformation. The structural reorganization of cylindrical micelles of the hexagonal

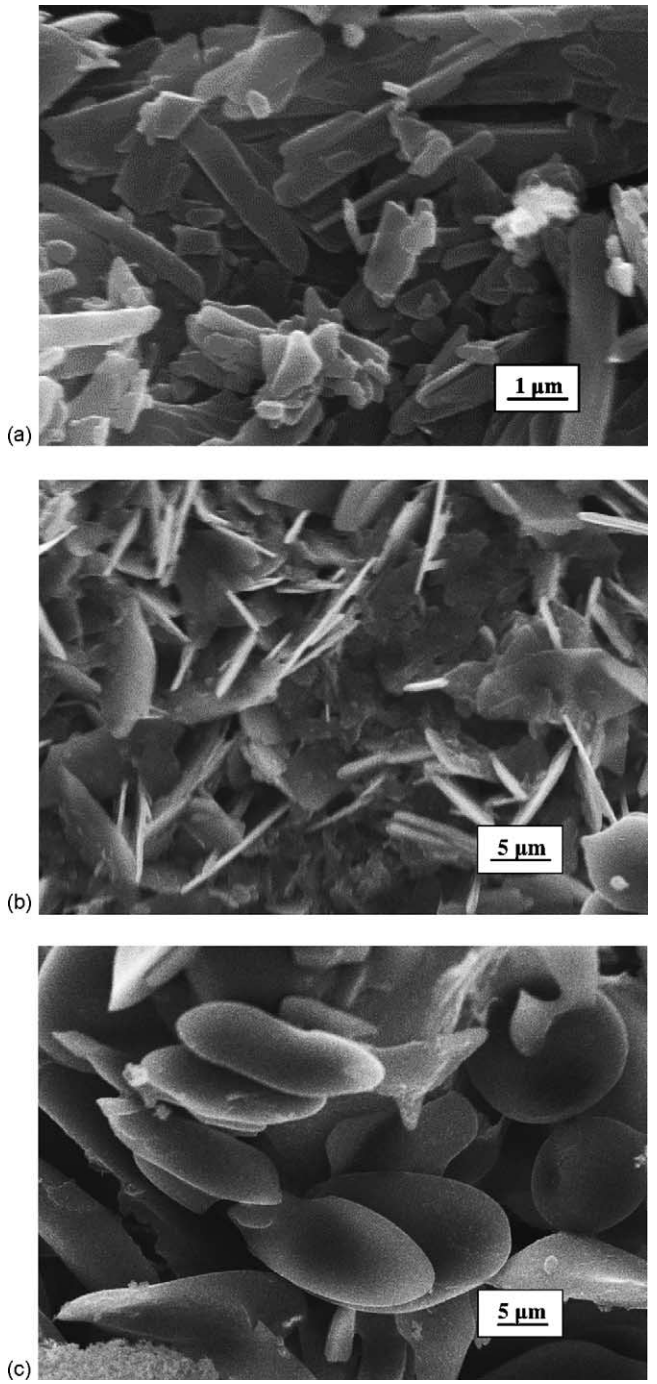

Fig. 3. SEM images of as-synthesized (a) lamellar, (b) hexagonal and (c) cubic mesoporous VPO phases prepared using $CH_3(CH_2)_{15}(CH_3)_3Br$, $CH_3(CH_2)_{11}NH_2$ and $CH_3(CH_2)_{15}SO_3Na$ as surfactants, respectively.

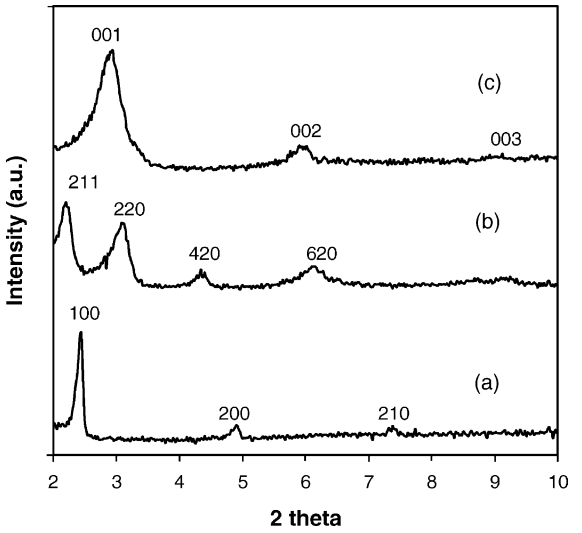

Fig. 4. XRD patterns of (a) as-synthesized hexagonal, (b) Soxhlet-extracted for 3 days (cubic) and (c) Soxhlet-extracted for 6 days (lamellar) mesoporous VPO phases, prepared using $CH_3(CH_2)_{11}OPO(OH)_2$ as a surfactant.

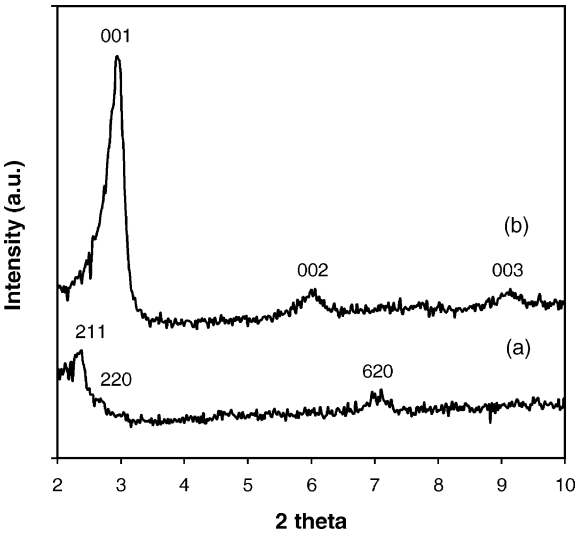

Fig. 5. XRD patterns of (a) as-synthesized cubic and (b) Soxhlet-extracted for 3 days (lamellar) mesoporous VPO phases, prepared using $CH_3(CH_2)_{15}NH_2$ as a surfactant.

structure into interconnected cylinders of the cubic structure during Soxhlet extraction may also be possible. This reorganization step was previously observed during aging process in the transformation of hexagonal MCM-41 to cubic MCM-48 [22,23]. Therefore, the change in the packing parameter is primarily responsible for the observed mesophase transformation. For even longer Soxhlet extraction times (Fig. 4c), the formation of the lamellar phase was observed. The XRD pattern for this sample shows three strong reflections corresponding to the (0 0 1), (0 0 2) and (0 0 3) planes of the lamellar phase [15]. Longer extraction times result in further swelling of the total volume of the surfactant chain by alcohol molecules which accumulate in the micelle periphery, increasing the "*g*" parameter close to its maximum value ($g = 1$), and leading to the lamellar phases. Longer Soxhlet extraction times (>10 days) resulted only in amorphous phases, indicating the collapse of the mesostructure. The cubic-to-lamellar phase transformation during Soxhlet extraction was also observed for the cubic mesostructured VPO phase synthesized using hexadecylamine structure-directing agent. The Soxhlet-extracted sample showed three strong XRD reflections corresponding to the (0 0 1), (0 0 2) and (0 0 3) planes of the lamellar phase (Fig. 5).

Thermal treatment in nitrogen. Phase transformations were observed after as-synthesized meso-VPO phases were treated in nitrogen at 673 K. Again, these mesophase transformations were explained by the changes in the surfactant packing parameter "*g*". Fig. 6 shows the XRD patterns for as-synthesized and N_2-treated meso-VPO phases synthesized using sodium hexadecane sulphonate as a surfactant. The as-synthesized sample displayed three reflections corresponding to the (0 0 1), (0 0 2) and (0 0 3) planes of the lamellar phase. After the thermal treatment in N_2, this sample showed three characteristic reflections corresponding to the (1 0 0), (1 1 0) and (2 0 0) planes of the hexagonal phase. The total volume (*V*) of the surfactant and cosolvent molecules decreased during the heat treatment due to the loss of water and ethanol leading to smaller "*g*" values and a transformation from a lamellar to a hexagonal structure with higher surface curvature. The lamellar-to-hexagonal transformation was observed for several samples using cationic and anionic surfactants. Nitrogen treatment led to the smallest "*g*" value configurations corresponding to more curved surfaces such as hexagonal or cubic. Fig. 7 shows the XRD patterns of as-synthesized hexagonal and N_2-treated cubic phases prepared employing dodecylamine as surfactant. The

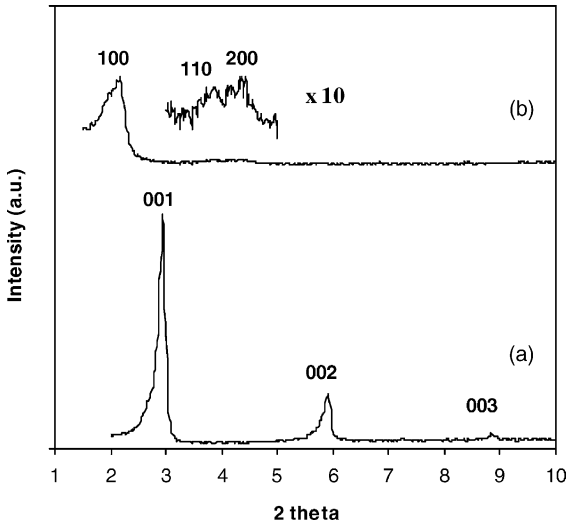

Fig. 6. XRD patterns of (a) as-synthesized lamellar and (b) thermally treated in N_2 at 673 K hexagonal mesoporous VPO phases prepared using $CH_3(CH_2)_{15}SO_3Na$ as a surfactant.

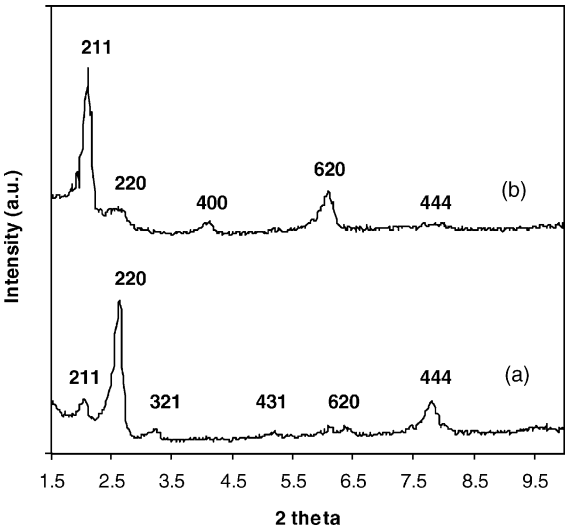

Fig. 8. XRD patterns of (a) as-synthesized cubic and (b) thermally treated in N_2 at 673 K cubic mesoporous VPO phases prepared using $CH_3(CH_2)_{15}NH_2$ as a surfactant.

as-synthesized mesophase showed the characteristic (1 0 0), (1 1 0) and (2 0 0) planes of the hexagonal phase. The N_2-treated sample showed three characteristic peaks corresponding to the (2 1 1), (2 2 0) and (4 3 1) planes of the cubic phase. As-synthesized cubic meso-VPO retained its structure after N_2-treatment at 673 K. However, the thermal treatment resulted in improved structural order manifested in the higher exposure of the (2 1 1) plane. Fig. 8 shows the XRD patterns of as-synthesized and N_2-treated cubic phases using hexadecylamine as a surfactant.

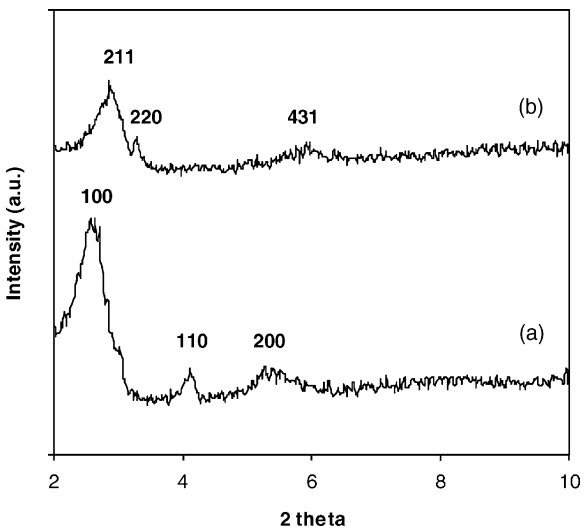

Fig. 7. XRD patterns of (a) as-synthesized hexagonal and (b) thermally treated in N_2 at 673 K cubic mesoporous VPO phases prepared using $CH_3(CH_2)_{11}NH_2$ as a surfactant.

Calcination in air. For as-synthesized meso-VPO phases calcined in air at 673 K, the original mesostructure was partially retained only when strong acidic self-assembly conditions were used. For V^{4+} source, the synthesis conducted under acidic pH conditions favored the formation of the VPO phases. In fact, the VPO phases are hydrolytically unstable at pH > 5 [24], which may explain the low phosphorus content and limited stability of the mesostructured VPO phases synthesized previously at pH ∼ 7.5 [13]. However, template removal increased the structural disorder in calcined samples (Fig. 9). Also, disordered and thermally unstable mesostructured VPO phases were observed for higher synthesis pH (>1). Interestingly, several catalytically active dense phases for *n*-butane oxidation to maleic anhydride such as $(VO)_2P_2O_7$ and γ-$VOPO_4$ were observed for these meso-VPO phases calcined in air. These dense phases were only observed when cationic surfactants (e.g. dodecyl, cetyl and mirystyl trimethyl ammonium bromides) were employed. Amoros and coworkers [14] observed these dense phases for their mesostructured

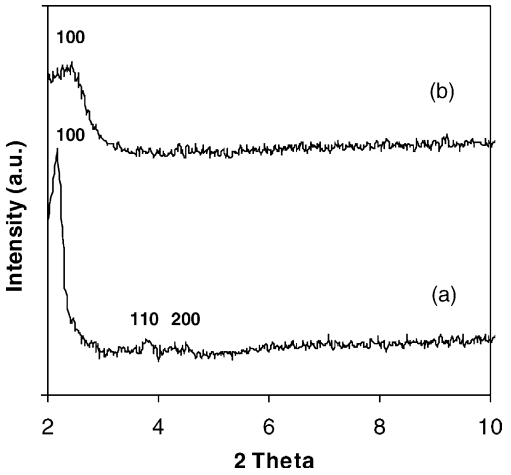

Fig. 9. XRD patterns of (a) as-synthesized and (b) calcined in air at 673 K mesoporous VPO phases prepared using $CH_3(CH_2)_{15}N(CH_3)_3Br$ as a surfactant.

oxovanadium phosphates after calcination in air and nitrogen at much higher temperature (973 K).

All meso-VPO phases synthesized using anionic and alkylamine surfactants, with the exception of the monododecyl phosphate samples, showed the P/V molar ratios in the 1.0–1.1 range. This slight excess of phosphate is optimal for achieving superior catalytic performance in the oxidation of *n*-butane to maleic anhydride [4,5]. For samples synthesized with monododecyl phosphate, the extra phosphate of the surfactant headgroup resulted in somewhat higher P/V ratios ~1.2–1.3. On the other hand, for the VPO phases synthesized using cationic surfactants, the P/V molar ratios slightly less than 1.0 were observed for the synthesis P/V ratio ~1.1, probably because some phosphate was associated with the cationic surfactant. However, in this case, a higher synthesis P/V ratio ($P/V = 1.4$) resulted in the meso-VPO phases with $P/V \sim 1.1$. The average oxidation state of vanadium in meso-VPO phases was determined by the double titration method [16]. The average vanadium oxidation state for all as-synthesized, Soxhlet-extracted and N_2-treated samples were in the +3.8 to +4.3 range, which is optimal for the selective oxidation of *n*-butane to maleic anhydride [4,16]. For air-calcined samples slightly higher oxidation states were observed (+4.1 to +4.5) probably due to oxidizing activation conditions (air at 673 K). The specific surface areas for the meso-VPO phases after surfactant extraction and thermal treatment were in the 10–60 m^2/g range. Although these areas are higher than those reported for conventional VPO catalysts (5–20 m^2/g), much higher surface areas were expected for these mesophases. Remaining occluded surfactant species as well as the presence of amorphous VPO regions were responsible for these relatively low surface areas. According to the XPS data (based on C1s), the air-calcined meso-VPO phases prepared using cationic surfactants contained ~30% of the original carbon present in the as-synthesized sample. Optimal post-synthesis conditions for complete surfactant removal and preparation of equilibrated VPO phases are currently under investigation.

4. Conclusions

Mesostructured VPO phases were prepared employing cationic, anionic and neutral surfactants under mild conditions and low pH. These mesophases displayed desirable vanadium oxidation states (+3.8 to +4.3) and bulk P/V molar ratios (~1.0) for the partial oxidation of *n*-butane to maleic anhydride. Interestingly, phase transformations of meso-VPO were observed during post-synthesis treatments. The Soxhlet extraction in ethanol led to mesophase transformations from the hexagonal-to-cubic-to-lamellar structure as a function of extraction time. Thermal treatment in N_2 led to lamellar-to-hexagonal and hexagonal-to-cubic transformations. These transformations were explained by the changes in the surfactant packing parameter *g*. To the best of our knowledge, this is the first time that these mesophase transformations are observed in the VPO system. Air-calcined samples showed mesostructured VPO phases with improved thermal stability and catalytically active dense phases for *n*-butane oxidation to maleic anhydride, namely $(VO)_2P_2O_7$ and γ-$VOPO_4$. These novel VPO phases represent promising catalytic systems for the partial oxidation of *n*-butane. Future studies will address the catalytic properties of these novel phases in selective alkane oxidation reactions.

Acknowledgements

The authors would like to thank Mr. A.M. Hirt (Materials Research Laboratories, Inc., Struthers, OH)

for the XPS data. This work was supported by the University of Cincinnati Research Council and the Wright-Patterson AFRL/DAGSI grant.

References

[1] F. Trifiro, Catal. Today 21 (1998) 41.
[2] M.M. Bettahar, G. Constentin, L. Savary, J.C. Lavalley, Appl. Catal. 145 (1996) 1.
[3] M.M. Lin, Appl. Catal. 207 (2001) 1.
[4] G. Centi, Catal. Today 5 (1993) 16.
[5] V.V. Guliants, J.B. Benziger, S. Sundaresan, I.E. Wachs, J.M. Jehng, J.E. Roberts, Catal.Today 28 (1996) 275.
[6] C.T. Kresge, M.E. Leonowicz, W.J. Roth, J.C. Vartulli, J.S. Beck, Nature 359 (1992) 710.
[7] J.S. Beck, J.C. Vartuli, W.J. Roth, M.E. Leonowicz, C.T. Kresge, K.D. Schmitt, C.T.W. Chu, D.H. Olso, E.W. Sheppard, S.B. McCullen, J.B. Higgins, J.L. Schlenker, J. Am. Chem. Soc. 114 (1992) 10834.
[8] F. Schuth, Chem. Mater. 13 (2001) 3184.
[9] D.M. Antonelli, Micropor. Mesopor. Mater. 30 (1999) 315.
[10] G.G. Janauer, A. Dobley, J. Guo, P. Zavalij, M.S. Whittingham, Chem. Mater. 8 (1996) 2096.
[11] V. Luca, J.M. Hook, Chem. Mater. 9 (1997) 2731.
[12] T. Abe, A. Taguchi, M. Iwamoto, Chem. Mater. 7 (1995) 1429.
[13] T. Doi, T. Miyake, Chem. Commun. (1996) 1635.
[14] J.E. Haskouri, M. Roca, S. Cabrera, J. Alamo, A. Beltran-Porter, D. Beltran-Porter, M.D. Marco, P. Amoros, Chem. Mater. 11 (1999) 1446.
[15] N. Mizuno, H. Hatayama, S. Uchida, A. Taguchi, Chem. Mater. 13 (2001) 179.
[16] B.K. Hodnett, P. Permanne, B. Delmon, Appl. Catal. 6 (1983) 231.
[17] Q. Huo, D.I. Margolese, U. Clesla, P. Feng, T.E. Gier, P. Sieger, R. Leon, P. Petroff, F. Schuth, G.D. Stucky, Nature 368 (1994) 317.
[18] J.N. Israelachvili, D.J. Mitchell, B.W. Ninham, J. Chem. Soc., Faraday Trans. 2 72 (1976) 1525.
[19] Q. Huo, D.I. Margolese, G.D. Stucky, Chem. Mater. 8 (1996) 1147.
[20] Q. Huo, R. Leon, P.M. Petroff, G.D. Stucky, Science 268 (1995) 1324.
[21] Q. Huo, J. Feng, F. Schuth, G.D. Stucky, Chem. Mater. 9 (1997) 14.
[22] C.A. Fyfe, G. Fu, J. Am. Chem. Soc. 117 (1995) 9709.
[23] K.W. Gallis, C.C. Landry, Chem. Mater. 9 (1997) 2035.
[24] V.V. Guliants, J.B. Benziger, S. Sundaresan, Chem. Mater. 6 (1994) 353.